ATLAS NOTE

August 3, 2013

Performance of resistive micromegas with VMM1 readout

J. Connors[a], N. Felt[a], M. Franklin[a], P. Giromini[a,b], A. Hussain[a]

[a]*Harvard University, Cambridge, Massachusetts 02138*
[b]*Laboratori Nazionali di Frascati, Istituto Nazionale di Fisica Nucleare, Frascati, Italy*

Abstract

We present a study of the VMM1 readout electronics using a resistive-micromega v2.0 prototype and a collimated ^{55}Fe source. We report a number of baby hiccups and shortcomings, some of which had yet to be noticed. This is understandable as the VMM1 is the first version of a quite sophisticated chip. In addition to this, the VMM1 charge/shaping amplifiers integrate only a fraction of the total charge induced on the x electrode by ionizing particles. This results in a micromega gain that is a factor of four smaller than what it is assumed in the NSW TDR. MIPs produce signals of the order of $3 - 5$ fC per x strip, awfully close to or below the present VMM1 thresholds. We propose to add an additional charge-integration scale with a gain of $\simeq 50$ mV/fC to mitigate this problem.

1 Detector description and experimental setup

The performance of the resistive-micromega v2.0 prototype is described in Ref. [1]. The amplifying gap of this prototype, shown in Fig. 1, is 128 μm thick. The cathode is a woven stainless steel mesh with 400 lines/in and a wire thickness of 18 μm. The mesh is kept at the 128 μm distance from the anode by a matrix of Pyralux pillars with 400 μm diameter and spaced by 2.5 mm in the x and y direction. The anode consists of resistive ribbons 35 μm thick, 100 mm long in the x direction, 180 μm wide, and with a 250 μm pitch. Each resistive strip is connected to ground with a 45 MΩ resistor. The resistance of each strip is 100 MΩ/cm. The 70 μm gaps between resistive strips are not filled with insulator. The resistive

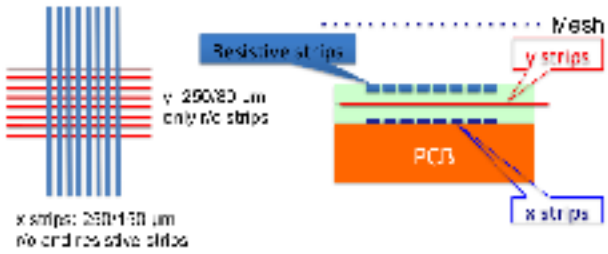

Figure 1: Resistive chamber sketch. Readout strip layout (left): the bottom x-readout strips are parallel to the resistive strips and orthogonal to the y-readout strips. Vertcal cross section (right). The figure is reproduced from Ref. [2].

layer is built on top of the y-readout electrode. The y electrode consists of 18 μm thick copper strips, 80 μm wide, with a 250 μm pitch and 10 cm long in the y direction. The y readout is separated from the resistive anode by a 64 μm layer of photo-imageable cover-lay. A similar cover-lay separates the y readout from the x readout which consists of 18 μm thick copper strips, 200 μm wide, with a 250 μm pitch, and 10 cm long in the x direction. The y readout is built on top of a 1 mm thick FR4 board, copper cladded and grounded on the opposite side. The 5 mm drift gap is built on top of the amplifying gap.

For these measurements, we use a 93% Ar + 7% C02 gas mixture. Voltages are supplied by a CAEN N1470 HV power supply. The drift voltage is set to -200 V, the mesh is at ground, and the resistive anode is set to 545 V. As shown in Ref. [1], the breakdown voltage of this detector due to spontaneous sparks is 560 V, but decreases to 540 V when irradiating the micromega with a rate of 1 kHz/cm^2 [1]. It is worth noting that we operate the detector at a voltage slightly higher than the breakdown voltage in a high rate environment. When lowering the voltage from 545 to less than 540 V, the detector gain decreases by a factor $F_{HR} = 0.7 - 0.8$.

We use a collimated ^{55}Fe source which illuminates 64 x and y readout strips off the chamber center. We derive the gain of the chamber from the charge corresponding to the 6 KeV line of the ^{55}Fe source assuming that a 6 KeV photon converted inside the drift gap produces 300 ionization electrons. As a reference, we measure the ^{55}Fe charge collected by all x (or y) strips with a ORTEC 142C charge preamplifier followed by a ORTEC 472A shaping amplifier set to a 1 μs shaping time. Then, we measure the charge collected by the 64 strips using one Arizona's card, hosting the VMM1 chip, connected to the VMM1 control and digitizer card [3].

The enable/stop to the digitizer card, in the following referred to as the trigger, is provided by the ^{55}Fe signals induced on the mesh, preamplified with a Canberra 1406 followed by a Lecroy 612A amplifier, the output of which is discriminated with a Lecroy 821D and converted to a TTL signal with an ORTEC 416A gate generator. Because the input of the 1406 preamp is decoupled with a 2 nF capacitance, comparable to that of the amplifying gap, only 70% of the produced charge is drained out of the micromega. Without this trigger penalty, all measured gain and charges at the readout electrodes would

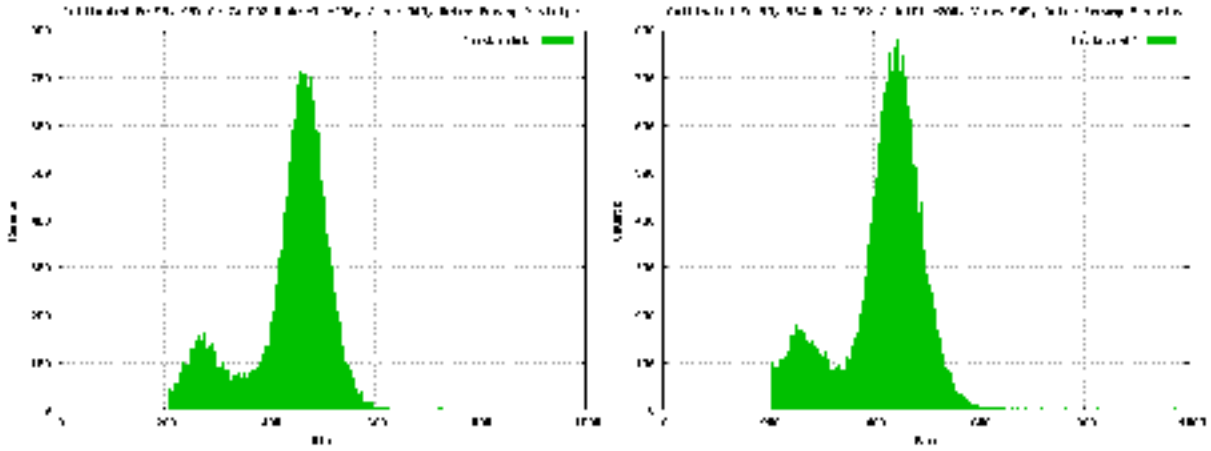

Figure 2: Charge distribution (arbitrary units) of the signals induced by the Fe^{55} source on all (left) x and (right) y electrodes read by a single 142C preamp.

be larger by a factor $F_{TP} = 1.44$. The peak of the ^{55}Fe charge integrated at the mesh is 300 fC. The trigger threshold is 100 fC. For lower thresholds, the noise produced by the VMM readout and picked up by the mesh induces trigger oscillations.

2 Results using a single charge amplifier

Figure 2 shows the ^{55}Fe spectra seen on the readout electrodes using the 142C preamplifier. The 6 KeV peaks corresponds to a charge of 290 fC and to a detector gain of 6050. After correcting for the factor $F_{TP} = 1.44$, the above numbers are consistent with what reported in Ref. [1], in which the entire detector was illuminated by the ^{55}Fe source. The charge integrated by the 142C preamp at the x and y electrodes will be used to benchmark the VMM1 performance.

3 VMM1 calibration

The VMM1 chip offers the possibility of calibrating the gain and pedestal of each shaping amplifier. This is achieved by enabling a 1.2 pF test capacitor for each channel. A voltage step, controlled by the onboard pulser DAC and test clock, is sent to any combination of enabled channels.

For each channel, the ASIC chip contains an analog section with a selectable-gain charge preamplifier and a high-order DDF (Delayed Dissipative Feedback) shaper with a peaktime selectable from 25 to 200 ns. The output of the shaping amplifiers can be monitored one channel at the time. The shaping amplifier is followed by a discriminator with a threshold adjustment common to all channels. The possibility is provided to adjust individually the threshold of each channel with a full range of 10 mV. This fine adjustment is at the moment ineffective since, as we will show later, the thesholds vary by as much as 50 mV from channel to channel.

The first integrated signal above threshold generates the ART signal of a detected event. We use the option that any channel over threshold enables also the acquisiton of its neighboring channels. The output of the shaping amplifier is followed by a peak detector, the voltage output of which, referred to as the PDO, is stored until digitized. The detection of a peak starts the TAC ramp for this channel. All TAC ramps are stopped by the trigger generated from the mesh signal. The TAC voltage, referred to as TDO, is also stored until read out together with the PDO and the channel address. Upon a trigger arrival, the stored PDO and TDO values are multiplexed to the digitizer card and recorded with a LabView

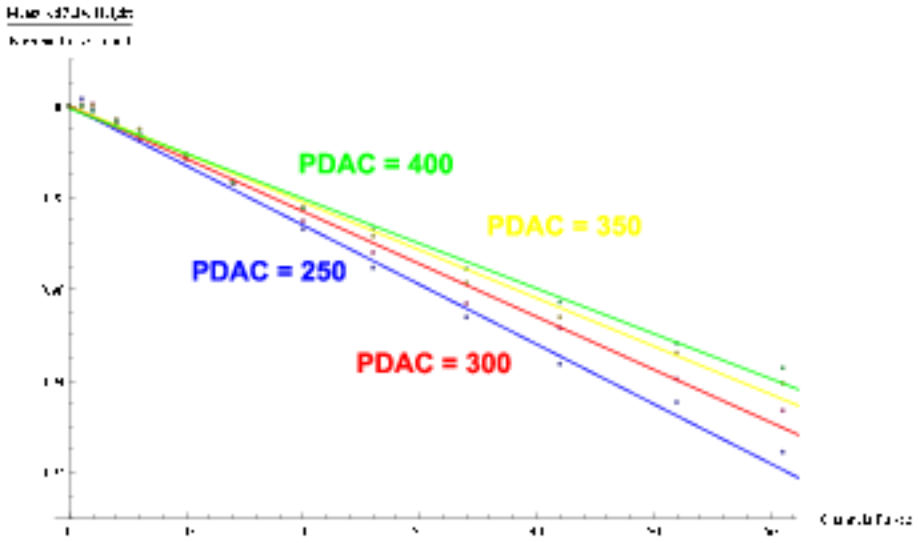

Figure 3: Fraction of charge injected into a given channel as a function of the number of channels pulsed simultaneously for four different DAC values indicated by the PDAC labels. When all 64 channels are pulsed, the loss of injected charge is 8% for DAC=250 and 6% for DAC=400.

program [3]. This concise description does not do justice to all work and skill that went into designing the VMM1 system, but it is a necessary primer to describe the difficulties ahead.

We run the chip with a nominal TDO scale of 1 V/μs and a PDO gain of 9 mV/fC. We choose a 200 ns peaking time, but have also studied the response of the x electrodes using peaking times of 50 and 100 ns. When comparing measurements, it is necessary to keep in mind that the 200 ns peaking time corresponds to 120 ns of shaping time in the ORTEC 472A amplifier.

We measure the PDO pedestals and gains (mV/fC) of all 64 channels simultaneously by using voltage steps generated with four different DAC values (250, 300, 350, and 400). Voltage steps do not correspond exactly to the DAC values and have been measured with a scope using the monitor channel. If the relation between DAC value and step voltage varies from chip to chip, the calibration of the NSW electronics will become a major hassle.

The second minor difficulty is that, for a given DAC value, the charge injected into a given amplifier depends on the number of pulsed channels. In principle, it should be easy to correct this effect by looking at the digitized-PDO value as a function of the number of pulsed channels. Unfortunately, as shown later, there are appreciable leaks of the stored PDO (and TDO) voltages, and the digitized values significantly depend on the time at which the digitization occurs which in turn depends on the number of to-be-digitized channels. This leakage rate has to be mitigated for two reasons. The first is that calibration constants, such a gains and pedestals, cannot depend on the event configuration, such as the multiplicity or the amount of deposited charge. The second is that, since both the voltage leak and the pulser drop depend on the number of pulsed channels, it will be impossible to calibrate the NSW electronics. For now, we have measured the injected-charge drop as a function of the number of pulsed channels by looking at the shaping amplifier output on the monitor channel for several different DAC values (see Fig. 3).

As anticipated earlier, after having corrected for the pulser-drop effect, we still find that the value of the digitized PDO depends on the number of pulsed channels. Having noticed that the digitized-PDO value of a given channel depends on the number of preceding channels being read-out, but not on the number of following channels, we concluded that the stored PDO voltages leak. While this leakage was

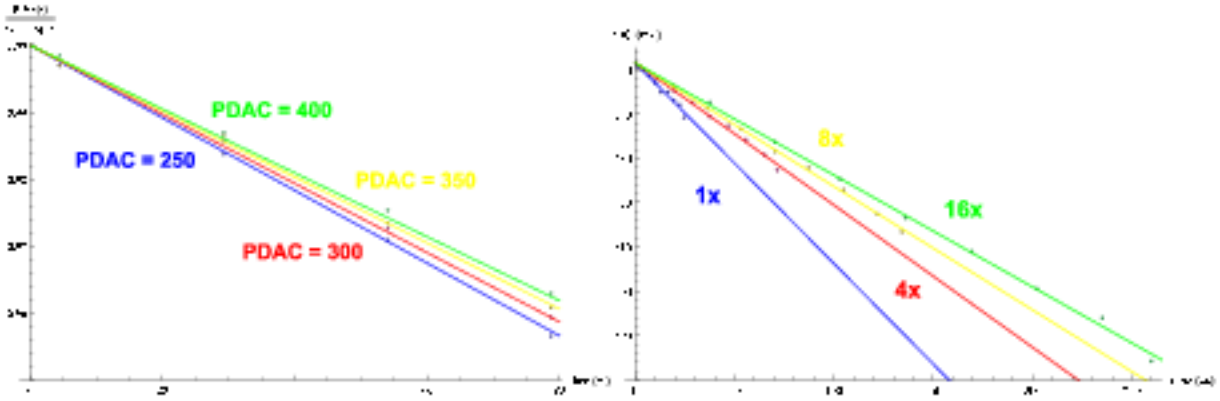

Figure 4: Left: the fractional decrease of the digitized-PDO value as a function of the digitization delay for different DAC values. Right: the decrease of the digitized-PDO value as a function of the digitization delay for different digitization samplings. The label 1x means that a PDO is digitized once in 500 ns, 16x means that it is digitized 16 times in 8 μs.

simulated to be at most 0.15 mV/μs [4], we observe leakage rates as large as 1.0 mV/μs. As shown by Fig. 4, the value of the digitized PDO depends on the time at which the channel is digitized. In the present setup, in which the VMM1 chip and the digitizer are separated, it is customary to improve the digitization accuracy by sampling 16 times the PDO of each channel, with each digitization cycle lasting 500 ns. This, in addition to a 250 ns settling time, means that each channel requires 8.25 μs to be read-out, after which the VMM1 multiplexer is advanced to the next fired channel. Channels are digitized in order of channel number, so that higher channels are increasingly mismeasured. An initial fix is to sample each channel only once, taking just 750 ns to advance the multiplexer. The RMS noise increases from 2.1 mV to 2.8 mV and this can be tolerated given the many additional sources of much larger errors we will encounter.

As shown by the right histogram in Fig. 4, an increase of the frequency at which the multiplexer is advanced produces an increase of the leakage rate. As shown by the left histogram in Fig. 4, the leakage rate also depends on the value of the stored PDO voltages. As shown by Fig. 5, the leakage rate varies appreciably from channel to channel. In summary, all these facts seem to indicate that the leakage rate depends strongly on the power used by the ASIC for a given event configuration [1].

Since ^{55}Fe signals light up a large and variable number of strips, each with a variable amount of charge, the leakage problem cannot be resolved unambiguously. For now, we use the 1x sampling and apply a correction as a function of the readout time, $t_{readout}$, using the average of the voltage-leakage rate over all channels and over all expected initial charges. When digitizing each channel once (1x sampling), the average leakage rate is measured to be 0.1%/μs. The readout time of a given channel is

$$\begin{aligned} t_{readout} &= t_{samp}\left(N_{pretck} + \frac{250 + 500\cdot(N_{samp}+1)/2}{t_{samp}}\right) \text{ (ns) with,} \\ t_{samp} &= (250 + 500\cdot N_{samp})\text{ (ns),} \end{aligned} \tag{1}$$

where N_{samp} is the number of times each channel is digitized and N_{pretck} is the number of channels digitized before. Figure 6 shows the pedestals and gains of the 64 VMM1 channels without corrections, with only the pulser-drop correction, and with both leakage and pulser-drop corrections. Pulser-drop corrections yield higher gains and pedestals, while leakage corrections increase gains and pedestals of

[1] As a side note, breathing close but not too close to the ASIC changes dramatically gains and pedestals. We have fixed the problem by increasing the ASIC heat capacitance with a 1" thick aluminmum heat sink as large as the chip.

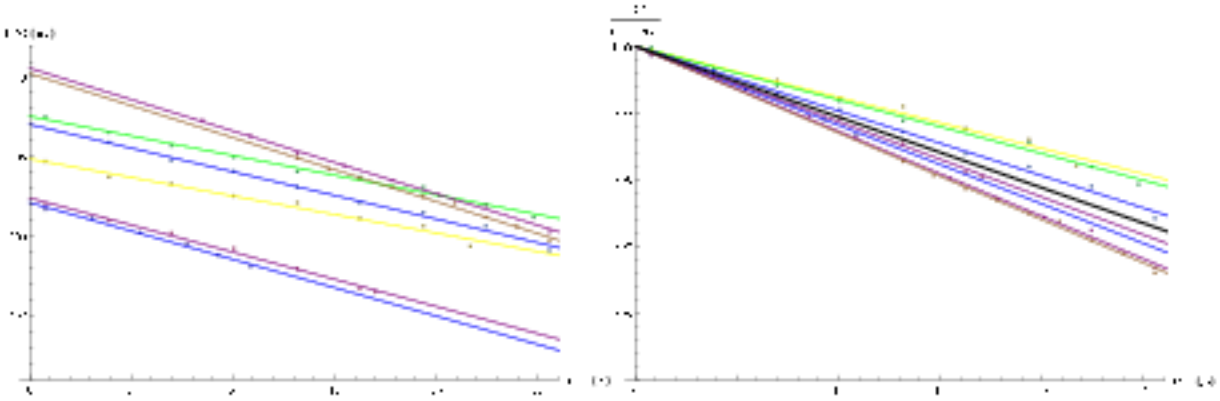

Figure 5: Left: digitized-PDO values as a function of the digitization time for seven randomly-selected channels injected with the same charge. The spread of the PDO values at t=0 corresponds to the variation of pedestals and gains. Right: fractional decrease of the digitized-PDO value for the seven channels as a function of time. The average of the various slopes (black line) is used to correct for the leakage as a function of time. This average slope is the same as the average of the slopes for different DAC values.

higher channels more. Calibrations of the VMM1 chip connected to the x or y electrodes are compared in Fig. 7. Lastly, calibrations of the VMM1 chip connected to the x strips for different peaking times are shown in Figs. 8 and 9. Only PDO gains and TDO pedestals depend on the peaking time.

We have also calibrated pedestals and TAC slopes of the digitized TDO by pulsing all channels simultaneously through the 1.2 pF test capcitances. We use the test pulse to start the TAC ramp, and the TDO is calibrated by generating TAC enable pulses of vaying lengths, the falling edge of which is the common TAC stop signal. We use enable pulse lengths of 300, 550, 800, 1050, and 1300 ns. The stored TDO voltages also leak. However, the average leak rate, 0.03%/μs, is appreciably smaller than that of the PDO voltages. The digitized-TDO value is also corrected using the equation (1).

4 Study of the y electrode response

We have acquired 600000 ^{55}Fe decays using the y strips and a 200 ns peaking time. The digitized PDO and TDO values are corrected as explained in the previuos section. Signals on the readout electrodes are induced by the collection of the ion-electron pairs produced in the amplifying gap as well as from diffusion of the charge collected on the resistive strips. Since the y strips are orthogonal to the resistive strips, the charge diffusion induces a signal on a large number of them. On average, the ^{55}Fe signal is collected by more than 20 y strips. For each event, we calculate the barycenter of the charge deposited on the various y strips and the total charge deposition. Figure 10 shows the total charge and the total number of fired strips as a function of the barycenter posistion. The total charge and multiplicity decrease when the barycenter moves far away from the center since the signal is also collected by strips which are not read out. We apply a fiducial cut and accept only events whose barycenter is between strip 14 and strip 42.

The mesh structure in the left plot of Fig. 10 is caused by the fact that channels have quite different threshold values. As shown by Fig. 11, the mesh structure vanishes when applying an offline threshold of 10 fC to all channels. The distribution of the event barycenters in shown in Fig. 12 before and after applying the 10fC offline theshold. Spikes in the left distribution are caused by the uneven thresholds of the VMM1 readout, and disappear after equalizing them offline. In the latter case, the inefficiency due to the pillars, spaced by 10 strips, becomes visible.

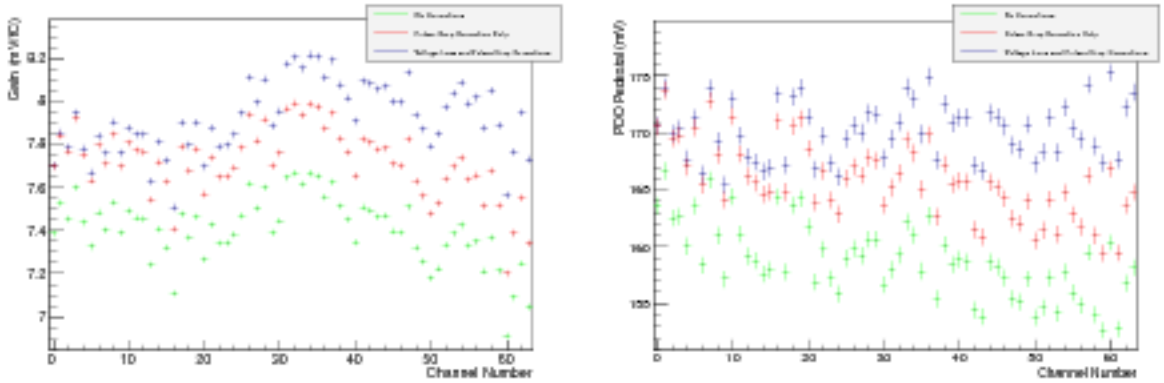

Figure 6: Distributions of (left) gains and (right) pedestals for each VMM1 channel with different levels of corrections applied.

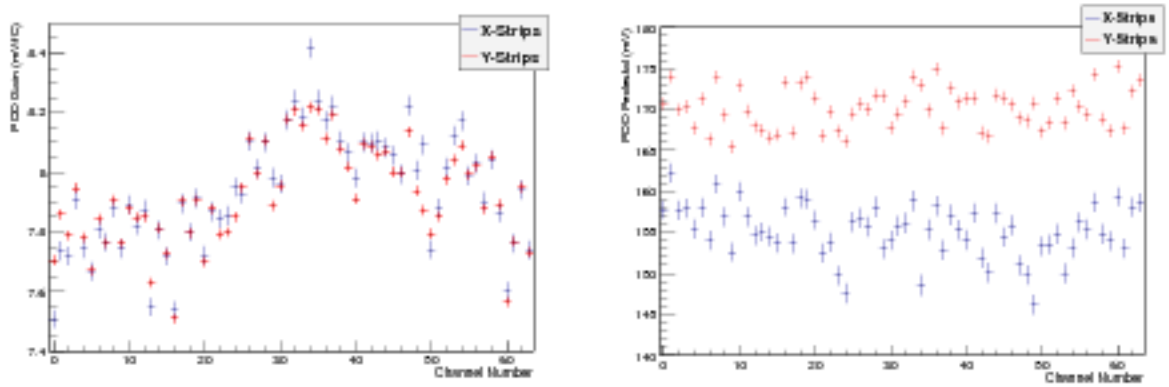

Figure 7: Distribution of the (left) gains and (right) pedestals of each VMM1 channel connected to the x and y strips. While the gains are similar, the pedestals are not because of the different capacitances of the x and y strips.

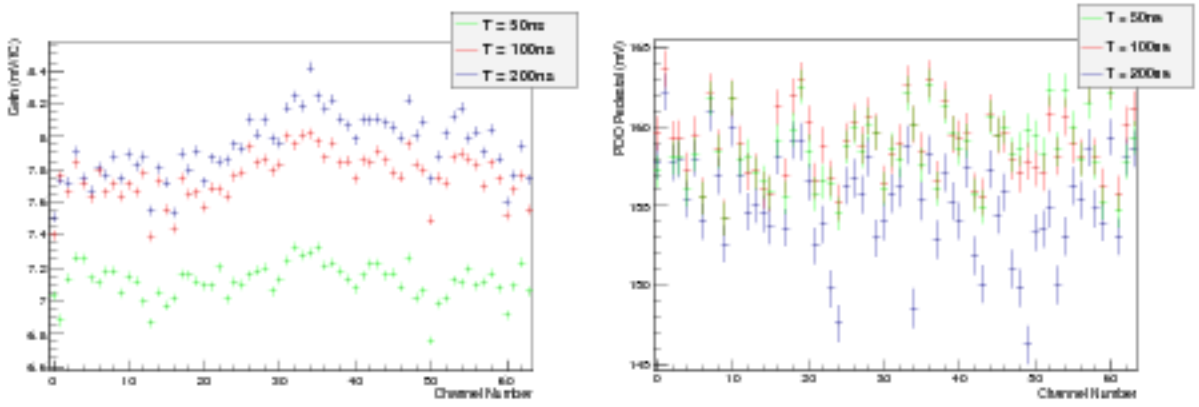

Figure 8: Distributions of (left) gains and (right) PDO pedestals of each VMM1 channnel connected to the x strips for different peaktimes. While pedestals are approximately independent of the peaktime, gains decrease with decreasing peaktimes.

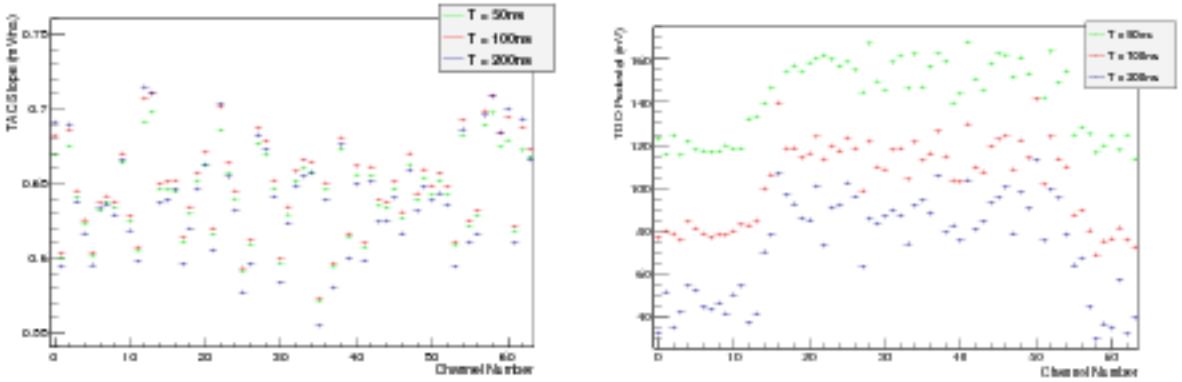

Figure 9: Distributions of the (left) TAC slopes and (right) TDO pedestals of each VMM1 channnel connected to the x strips for different peaktimes. The TAC slopes are almost independent of the peaktime, whereas, as expected, the pedestals decrease with increasing peaktimes.

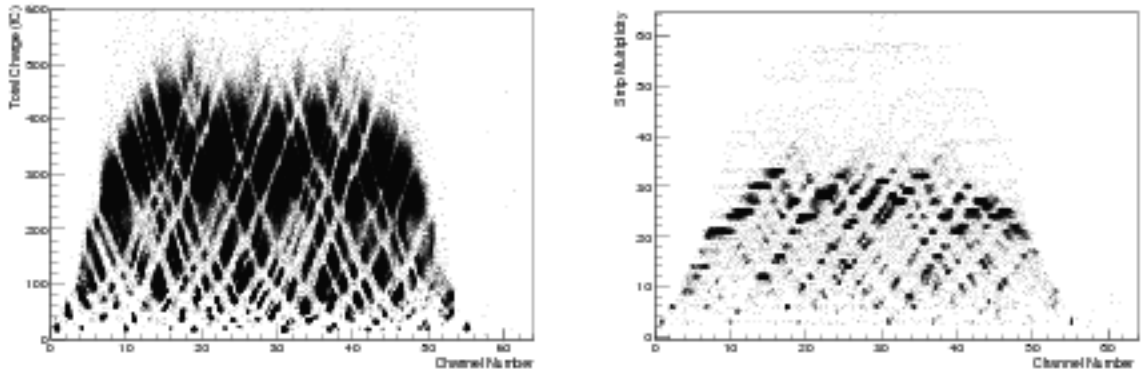

Figure 10: Distributions of the (left) total charge deposited by the ^{55}Fe source on the y strips and of the (right) y-strip multiplicity as a function of the y position of the charge barycenter. The strip pitch is 250 μm.

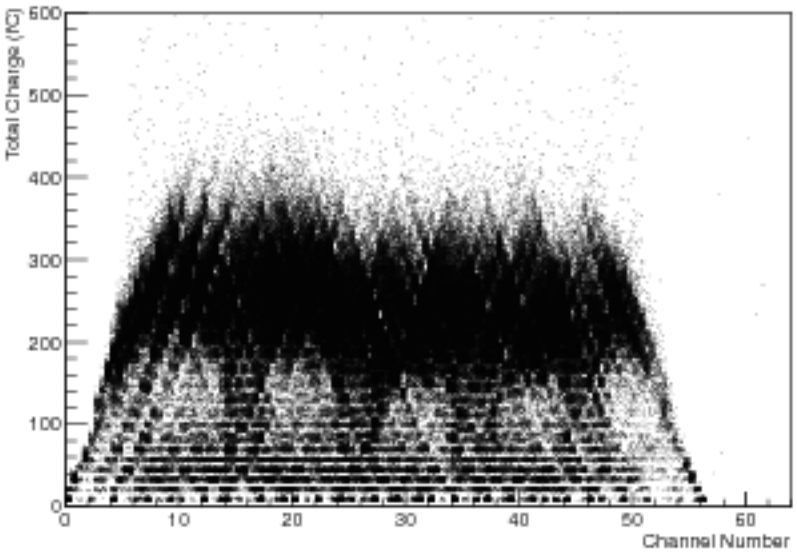

Figure 11: Distribution of the total charge deposited by the ^{55}Fe source on all y strips versus the y-position of the charge barycenter after a 10 fC offline threshold is imposed on each strip. The dark vertical bands, visible below 160 pC at channel numbers 16, 26, 36, and 46, correspond to the Pyralux pillars supporting the mesh.

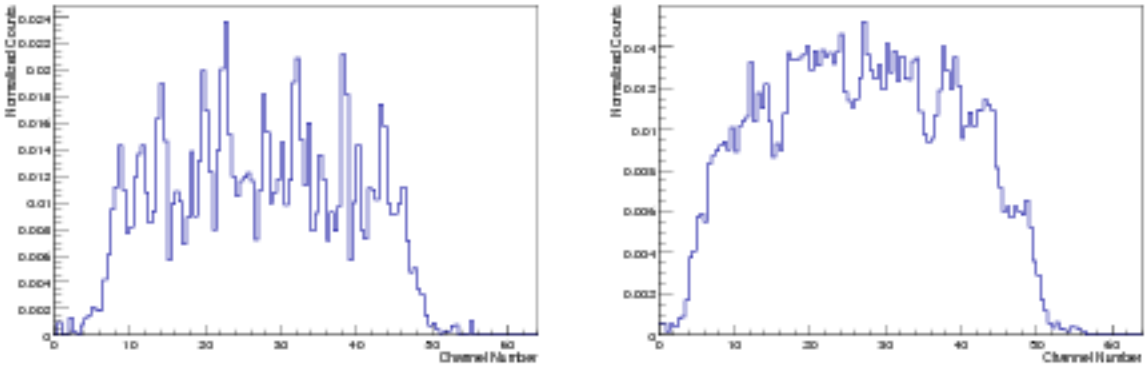

Figure 12: Distribution of the barycenters of ^{55}Fe signals collected by the y-strips before (left) and after (right) imposing a 10 fC offline threshold.

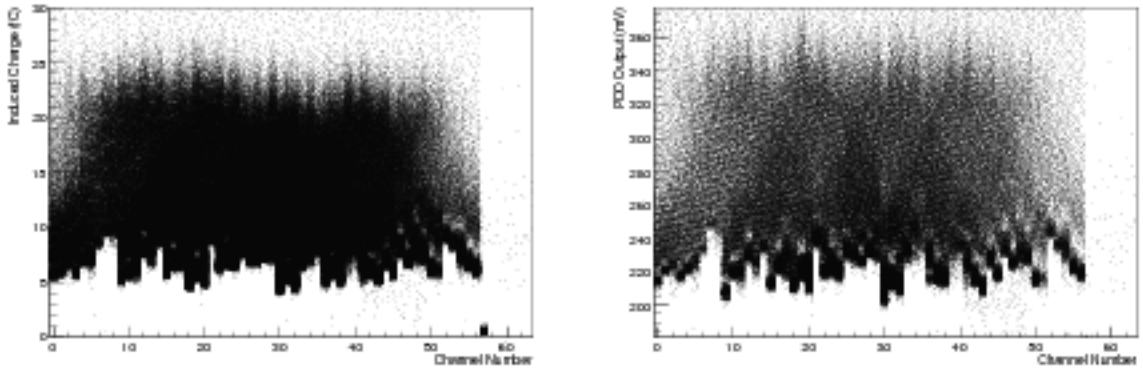

Figure 13: Distribution of the induced charges (left) and PDO values (right) for each y strip in all events.

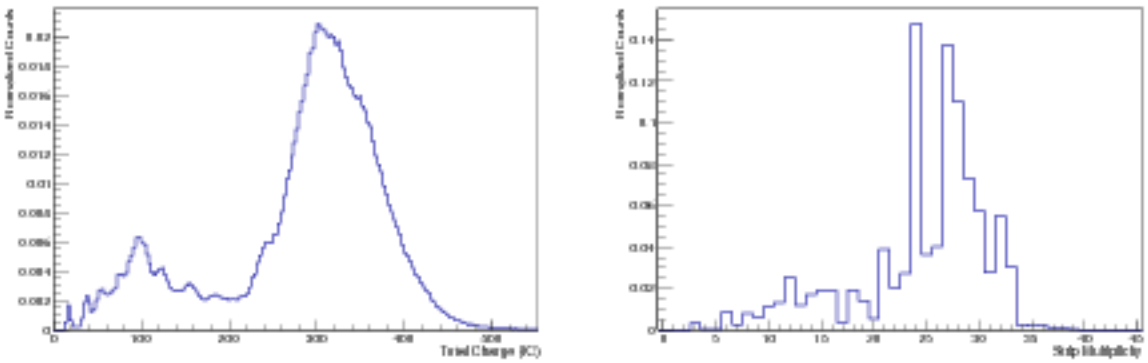

Figure 14: Left histogram: distribution of the total charge induced on the y strips by ^{55}Fe decays. Right histogram: strip multiplicity for the same events. In average, 23 strips light up in one event.

In Fig. 13, the distribution of the charge and PDO voltage seen by each channel in all events shows the thresholds of each channel both in fC and mV. The minimum common threshold at which all channels are working properly is approximately to 210 mV. The effective threshold for the different channels varies as much as 40-50 mV, making the fine threshold trimming of up to 15 mV quite ineffective.

The distribution of the charge due to ^{55}Fe decays, reconstructed after applying the fiducial cut, is shown in Fig. 14. In comparing to Fig. 2, one notes the distorsions of the spectrum caused by the approximate voltage-leakage corrections and the uneven thresholds of the different VMM1 channels. The ^{55}Fe peak corresponds to 300 fC, matching the value obtained with the 142C preamp and yields a detector gain of 9000 including the $F_{TP} = 1.44$ correction factor. The strip multiplicity distribution is shown in Fig. 14 and the correlation between the collected charge and the strip multiplicity is shown in Fig. 15.

The average y-strip multiplicity is ~23 and corresponds to a 6 mm long charge deposition on the y electrode, 20 times longer that the ionization segments (0.3 mm) produced by ^{55}Fe decays. As already noted in [5], this size amplification is caused by the diffusion of the charge deposited on the resistive strips which induces signals on y strips further away from the ionization point at later times. This effect is illustrated by Fig. 16 in which the time difference between a strip in a cluster and the barycenter strip is plotted as a function of its y distance from the barycenter.

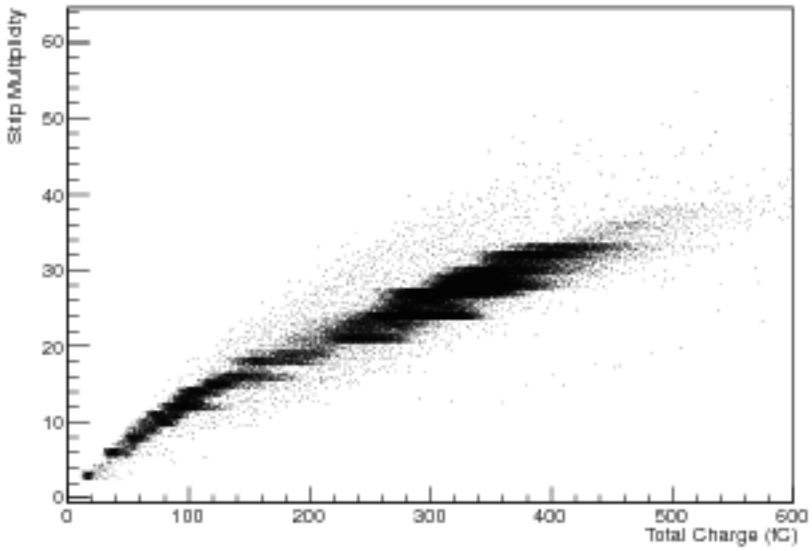

Figure 15: Distribution of the y-strip multiplicity as a function of the total charge induced by ^{55}Fe decays. As the total induced charge increases, so does the number of channels above threshold. This increase is largely due to the effect of the charge diffusing along the orthogonal resistive strips.

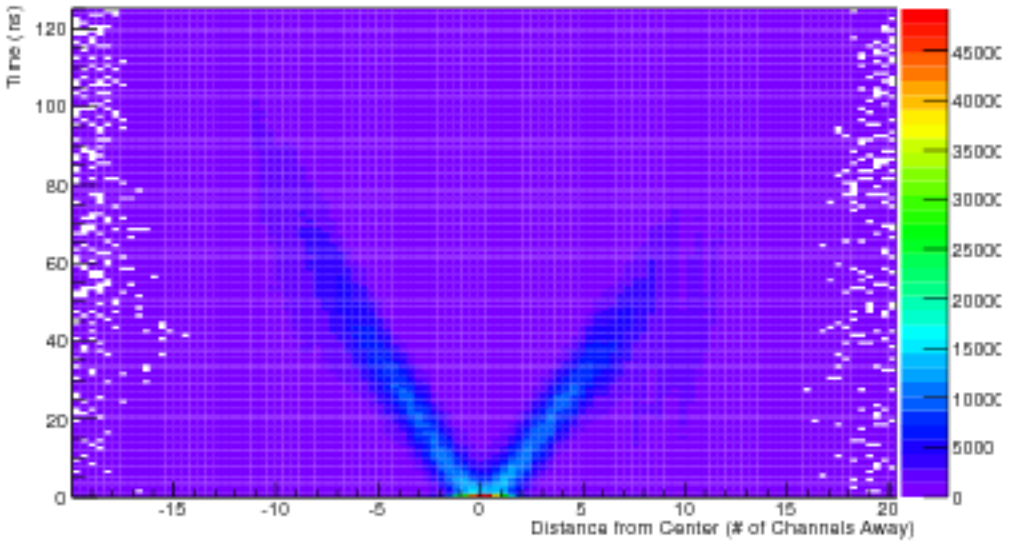

Figure 16: Density plot of the time difference between a strip in a cluster and the barycenter strip as a function of their respective distance. The V-shaped distribution is produced from ionization charge collected by the resistive strips diffusing along their length. The slope of the "V" is approximately 6 ns per strip.

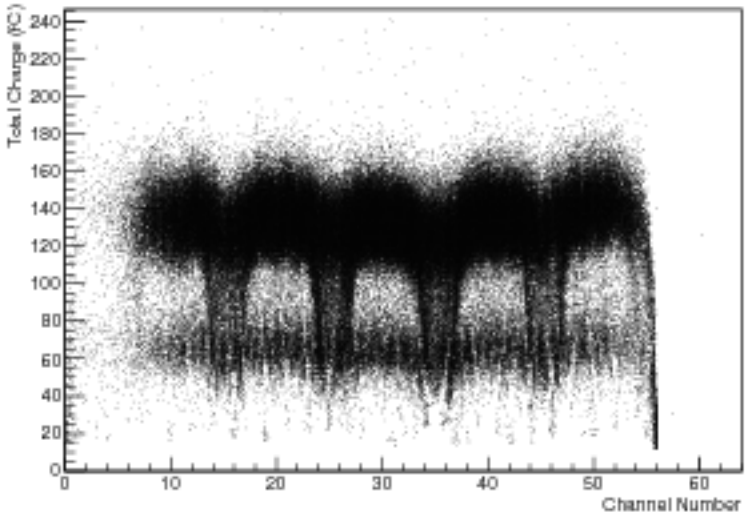

Figure 17: Distribution of the charge deposited on the x strips by ^{55}Fe decays as a function of the charge barycenter (measured in x-strip number). One can distinctly see the two black horizontal bands corresponding to the 6 KeV ^{55}Fe peak and the 3 KeV Ar escape peak. The vertical black bands around strip numbers 16, 26, 36, and 46 show the loss of efficiency due to the mesh-supporting pillars.

5 Study of the x electrodes

We have collected over 750000 ^{55}Fe decays with the x strips using three different peaking times of 50 ns, 100 ns, and 200 ns. The charge collected by the x strips is reconstructed as that of the y strips, including the voltage-leakage corrections. Figure 17 shows the total charge collected by the x strips versus their barycenter position. We apply a fiducial cut keeping only events with barycenters between strips 14 and 42. The distribution of event barycenters is shown in Fig. 18, and one clearly sees the inefficiency introduced by the pillars with are spaced by 10 strips.

The ^{55}Fe spectrum is shown in Fig. 19 for the three different peaking times. Not all charge induced on the x electrode is accounted for by the VMM1 peak detector. For a 200 ns peaktime, the 6 KeV peak corresponds to 130 fC instead of 290 fC, as integrated by the ORTEC 142 preamp. After correcting for the factor $F_{TP} = 1.44$, the charge collected by the x electrode is $Q = 31$ fC/KeV and the detector gain is $G = 3900$. For a 100 ns peaktime, $Q = 30$ fC/KeV and $G = 3600$; for a 50 ns peaktime, $Q = 26$ fC/KeV and $G = 3300$.

Micromegas built as the prototype v2.0 will not operate at voltages larger than 540 V in a high radiation environment. Using a 100 ns peaktime, required if a micromega trigger will be implemented, one expects to collect $Q = 21$ fC/KeV (a MIP deposits 1 KeV). The micromega gain, $G = 2500$, will be a factor of four smaller than what is assumed in the NSW TDR.

Figure 20 shows the strip multiplicity for the three different peaking times. The average strip multiplicity is $\simeq 4$ after taking into account the effect of the neighbor trigger. A MIP perpendicular to the detector deposits in average 5.2 fC per strip. A MIP with a 20 degree angle will deposit 3 fC per strip. This is below the threshold values which, as shown by Fig. 13, vary between 5 and 10 fC. Even assuming that VMM2 will allow a better equalization of the thresholds, the MIP signal is still awfully close to the threshold. A possible remedy is to add a charge-integration scale of $\simeq 50$ mV/fC so that a MIP signal will look like the ^{55}Fe decays we have studied.

Lastly, we verify the TOF resolution of the VMM1 electronics. Figure 21 shows the time difference

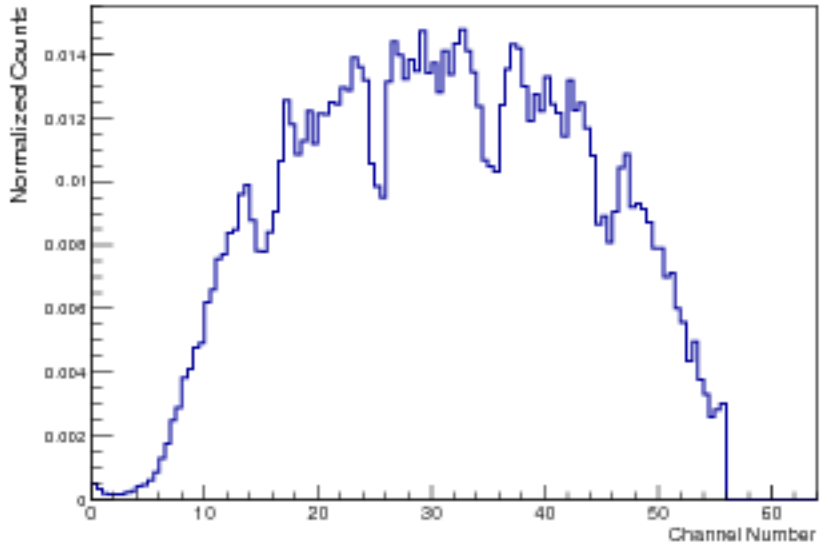

Figure 18: Distribution of the barycenters of the charge induced by ^{55}Fe decays on the x strips. The $\simeq$ 27% inefficiency caused by the pillars at channels 16, 26, 36, and 46 is much larger than the fraction of dead area created by the pillars ($\simeq$ 8%).

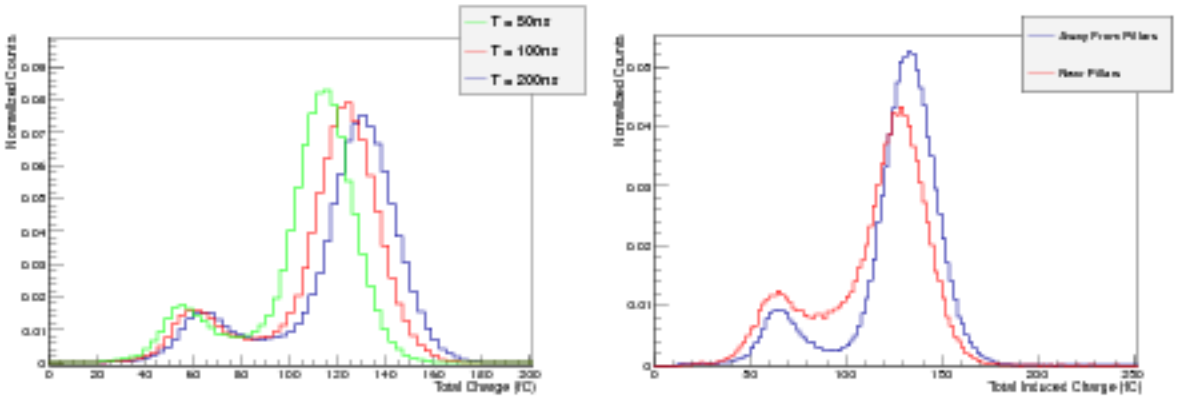

Figure 19: Left histogram: distribution of the total charge induced by ^{55}Fe decays on the x electrode for three different peaking times. For a 200ns peaking time, the 6 KeV main peak corresponds to ~130 fC. For shorter peaktimes, there is a 7% gain loss at 100 ns and 15% at 50 ns. Right histogram: distribution of the total charge induced by ^{55}Fe decays when the charge cluster lies in x- electrode regions covered or not covered by pillars.

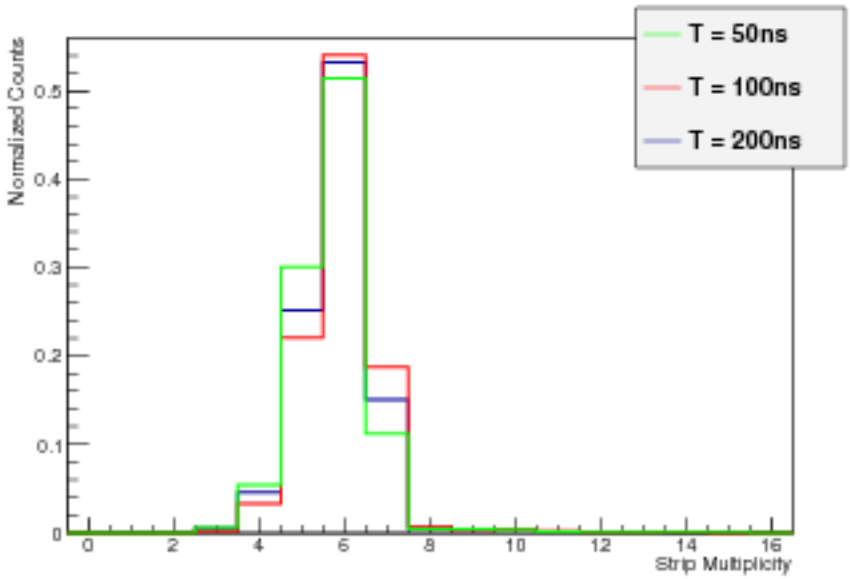

Figure 20: Distribution of the number of x strips fired by ^{55}Fe decays for three different peaking times. Since we acquired these data using the neighbor trigger option, on average only 4 strip signals are above threshold.

between the two strips with the highest charge in a cluster produced by ^{55}Fe decays. The RMS resolution of 6 ns is consistent with the measured TDO RMS noise of ~2.8 mV and TAC slope of 0.6 mV/ns.

6 Conclusions

We have studied the performance of the VMM1 electronics using a v2.0 prototype of resistive micromega and a ^{55}Fe source. We have found and describe in detail a number of technical issues, some of which have not been noticed before. This does not come as a surprise considering that VMM1 is the first version of a very sophisticated chip. The worst problems are the leakage of the stored PDO and TDO voltages, found to be much larger than what was simulated, and the uneveness of the thresholds. Apart from these effects, which will be likely mitigated in the next version of the chip, the VMM1 chip integrates only a fraction of the charge induced on the x strips. When using A 100 ns peaktime, the gain of the detector is four times smaller than what is assumed in the NSW TDR, and MIP signals will fall awfully close to the VMM1 lowest threshold. We propose to compensate this loss of integrated charge by implementing a new integration scale with a gain of $\simeq$ 50 mV/ fC in the next version of the chip.

References

[1] J. Connors *et al.*, ATLAS-UPGRADE-2013-023.

[2] M. Byszewsky and J. Wotschack, doi:10.1088/1748-0221/7/02/C02060

[3] The VMM1 readout cards were provided by Vinnie Polychronakos and Jessica Metcalfe who also made available the Labview programs used to acquire data and calibrate the readout chip. VMM1 details can be found at

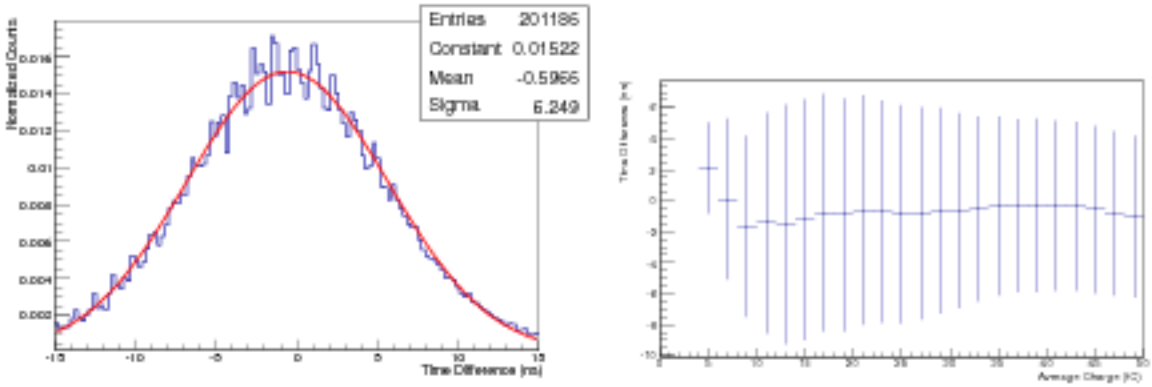

Figure 21: Left histogram: distribution of the time difference between the two x strips with the largest charge deposits in a cluster produced by ^{55}Fe decays. The right histogram show the average and RMS deviation of the same distribution as a function of the average charge of the two strips.

https twiki.cern.ch/twiki/pub/Atlas/NSWelectronics/VMM1_datasheet_v3a.pdf by G. De Geronimo et *al.*.

[4] private communication; we have discussed the leakage problem with G. De Geronimo at length.

[5] J. Connors *et al.*, ATLAS-UPGRADE-2013-019.